Plasma heating by ion gyro-scale blobs in the kinetic and fluid regimes

2013 Plasma Phys. Control. Fusion 55 055010

(http://iopscience.iop.org/0741-3335/55/5/055010)

Plasma Phys. Control. Fusion **55** (2013) 055010 (6pp) doi:10.1088/0741-3335/55/5/055010

Plasma heating by ion gyro-scale blobs in the kinetic and fluid regimes

P W Gingell[1], **S C Chapman**[1] **and R O Dendy**[1,2]

[1] Centre for Fusion, Space and Astrophysics, Department of Physics, University of Warwick, Coventry, CV4 7AL, UK
[2] Euratom/CCFE Fusion Association, Culham Science Centre, Abingdon, OX14 3DB, UK

E-mail: p.gingell@warwick.ac.uk

Received 23 November 2012, in final form 2 April 2013
Published 19 April 2013
Online at stacks.iop.org/PPCF/55/055010

Abstract
Strongly localized concentrations of plasma density ('blobs') are ubiquitous in the near-edge region of tokamak plasmas. They contribute significantly to heating and transport in that region, and therefore to overall energy confinement. The blob population may include some whose characteristic length scales are on the order of the ion gyro-scale, and cannot be resolved by contemporary diagnostics. Using simulations of ion gyro-scale blobs that include full ion kinetics, we perform the first comparison between the heating ability of ions in small, kinetic blobs and in larger, fluid ones. We find that, embedded in a flowing plasma, small scale blobs contribute more heating per ion than larger blobs, as a result of ion pick-up at the upstream blob-background boundary. This may result in significant excess plasma heating by an ion population that is not yet directly observable.

(Some figures may appear in colour only in the online journal)

1. Introduction

Coherent, propagating filamentary plasma structures, which appear in cross-section as 'blobs', are observed in the edge region of tokamaks [1–5]. Their role in the local physics is significant, notably their heating effect and their role in energy and particle transport in the edge plasma [6, 7], which is important for future experiments such as ITER [8]. Blob diameters extend down to ion gyro-scales, and some mechanisms for blob-driven heating arise from ion kinetic effects [9] on these scales. It is therefore important to understand how these effects, in combination, depend on plasma parameters, flow speeds, and blob characteristics. In tokamak edge plasmas [10], some blobs may be the poloidal projection of detached magnetic flux tubes, or ropes, that extend along the direction of the magnetic field. Polarising curvature drifts of ions and electrons give rise in the classic picture [11] to $\boldsymbol{E} \times \boldsymbol{B}$ radial blob motion. Models for blob transport and evolution relevant to magnetic confinement fusion have focused on fluid, multi-fluid and gyro-averaged kinetic descriptions, approached both analytically and numerically [12–19]. There have been successful simulations of blob creation via interchange-ballooning modes [13]. However, fully self-consistent ion kinetic simulations have only recently begun to be applied to the problem of blob evolution in tokamaks [9]. We consider small blobs on a range of spatial scales, from below to above the ion Larmor radius. The scale sizes that we consider are below that at which curvature driven interchange instability is known to be important [20], and the fluid-like behaviour is dominated by the K–H instability [21, 22].

Filamentary structures are also of interest in astrophysical plasmas as a means for transporting magnetic flux, plasma momentum and energy. In boundary layers of the Earth's magnetosphere, for example, this is observed to take place on ion kinetic scales [23–26] and has been the subject of kinetic simulations [27–29]. Finite Larmor radius effects are observed to be important in relation to small scale structures including comets [30–32], release experiments [33, 34] and elsewhere in planetary physics [35–41]. The generation of filaments and blobs on ion kinetic scales is thus ubiquitous in natural and laboratory plasmas. The importance of processes on ion kinetic scales in blobs in tokamak plasmas is thus an open question.

To address the physics of small blobs that may exist on scales comparable to the ion gyro-radius, we use here a hybrid treatment which self-consistently evolves the full ion kinetics without gyro-averaging, while modelling the electrons

as a massless fluid. First results [9] have shown that the interaction of blob ions with the background flow proceeds in a fundamentally different manner for blobs on fluid scales and ion kinetic scales. This raises the question whether the rate of heating of ions originating within blobs also depends on blob size. Hence our focus here is on the integrated effects of blob evolution on the plasma, rather than on phenomena associated with the evolution of individual blobs as in [9]. The impact of the multiple ion species present in a burning fusion plasma on these kinetic scale blobs has also not hitherto been explored. We investigate these questions by means of simulations which incorporate six-dimensional phase space particle-in-cell ion kinetics and an electron fluid. Our hybrid approach captures the nonlinear interaction between ion gyration and plasma inhomogeneity; cross-scale coupling between ion gyro-scale kinetic modes and fluid MHD-like modes; and non-Gaussian ion velocity distributions. It incorporates multiple distinct ion populations in velocity and configuration space.

Here we present the results of fully self-consistent ion kinetic simulations of small scale (kinetic) structures, representing proton and deuterium–tritium blobs with radius R_B ranging from ρ_p to $10\rho_\mathrm{p}$, where the background proton gyro-radius $\rho_\mathrm{p} = \sqrt{2m_\mathrm{p}kT_\mathrm{p}}/eB_0$. We find that smaller blobs, for which $R_\mathrm{B} \sim \rho_\mathrm{p}$, heat the plasma at a faster rate than their larger counterparts for which $R_\mathrm{B} \gg \rho_\mathrm{p}$. The mechanism for this heating is found to be a consequence of ion pick-up at the upstream edge of the blob, and of momentum transfer between internal vortices and the background flow. We establish how heating of blob ions scales with background flow speed, enabling the result to be generalized.

2. Simulations

The hybrid description [42] treats ions kinetically as particles whose trajectories respond in full 6D phase space to the Lorentz force. Electromagnetic fields are evolved self-consistently from Maxwell's equations and Ohm's law in the low frequency Darwin limit [43]. The model assumptions are: inertia-less electrons; $\boldsymbol{\nabla} \cdot \boldsymbol{E}$ negligible on length scales of interest, implying charge neutrality such that $en_\mathrm{e} = \sum_i q_i n_i$; collisionless plasma; and an ideal, isothermal electron fluid $\nabla \cdot \underline{\underline{P_\mathrm{e}}} = \nabla p_\mathrm{e} = kT_\mathrm{e}\nabla n_\mathrm{e}$. The full three-dimensional $\boldsymbol{E}$, $\boldsymbol{B}$ and $\overline{\overline{\boldsymbol{J}}}$ vector fields are advanced with second-order accuracy on a 2D grid in space (x,y) and in time. The hybrid approach and chosen geometry allow for the propagation of magnetoacoustic waves and the full resolution of ion gyration in the simulation plane.

The 2D grid of 960 cells in x and y is chosen with cell size $\Delta x = 3.75 \times 10^{-3}\,\mathrm{m} = 0.4\rho_\mathrm{p}$. The box size is chosen to be sufficiently large to capture the full evolution of the moving plasma blob and is typically $450\rho_\mathrm{p} = 320\rho_\mathrm{D} = 250\rho_\mathrm{T}$. The time step is determined by the CFL condition and is on the order of 10^5 time steps per ion gyro-period. We use sufficient particles per cell to fully represent the ion velocity distribution and a typical simulation employs 10^8 total computational particles, or roughly 100 particles per cell.

The simulations represent blobs as flux ropes with Gaussian spatial profiles of particle number density, with peak density five times the background n_0. Corresponding to the local density enhancement is a local depression in the magnetic field energy density, such that initially the system is in combined pressure equilibrium everywhere. The background plasma parameters are chosen to be approximately characteristic of edge conditions in a tokamak: $n_0 = 10^{19}\,\mathrm{m}^{-3}$, magnetic field $B_{z,0} = 0.4\,\mathrm{T}$, ion and electron temperature $T_0 = 4 \times 10^6\,\mathrm{K}$, and proton gyro-radius $\rho_\mathrm{p} = 8 \times 10^{-3}\,\mathrm{m}$. The background is initialized flowing transversely to the magnetic field at speed $u_\mathrm{flow} = 0.2v_\mathrm{A}$ for all simulations, where v_A is the background proton plasma Alfvén speed.

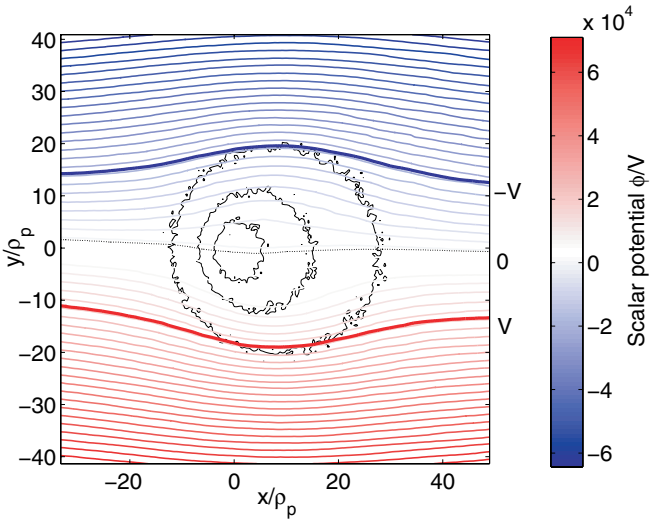

Figure 1. Contours of scalar potential ϕ (red and blue) and density (black) across a $10\rho_\mathrm{p}$ proton plasma blob at an early time $t = t_\Omega$ in the simulation, in the blob's initial rest frame. We highlight scalar potential contours which pass along the top and bottom edge of the blob, corresponding to a cross-blob potential difference consistent with $u_\mathrm{flow} = 0.2v_\mathrm{A}$ and $B_0 = 0.4\,\mathrm{T}$. Note that the gradient of the scalar potential is reduced inside the blob compared to the background flow, where the motional electric field is reduced.

Here, the background flow, which is in the x-direction, represents a vector combination of the velocity imparted to the blob in an approximately radial direction during its creation and the smaller velocity of the poloidal background flow within the LCFS. The y-coordinate is perpendicular to the x-coordinate and to $\boldsymbol{B}$ in this coordinate system. The background flow speed, which is sub-Alfvénic ($u_\mathrm{flow} = 0.2v_\mathrm{A}$), is chosen with a view to achieving significant temporal evolution given the spatial resolution required and the computational resource available. Here, the simulations are carried out in the initial rest frame of the blob. Conversely in the rest frame of the background flow, the blob initially moves transversely to the magnetic field with velocity $-u_\mathrm{flow}$.

In the classical picture, blobs in the SOL are subject to a radial $\boldsymbol{E} \times \boldsymbol{B}$ force resulting from a polarizing drift within the blob [11]. However, uncertainty exists in the range of positions at which blobs may be created [4, 10]. This uncertainty allows that some may propagate first through the confined plasma within the separatrix. We simulate the evolution of those blobs which are born and propagate first within the confined plasma, which are not subject to the polarizing drift and resulting radial force. The initial and boundary conditions include a

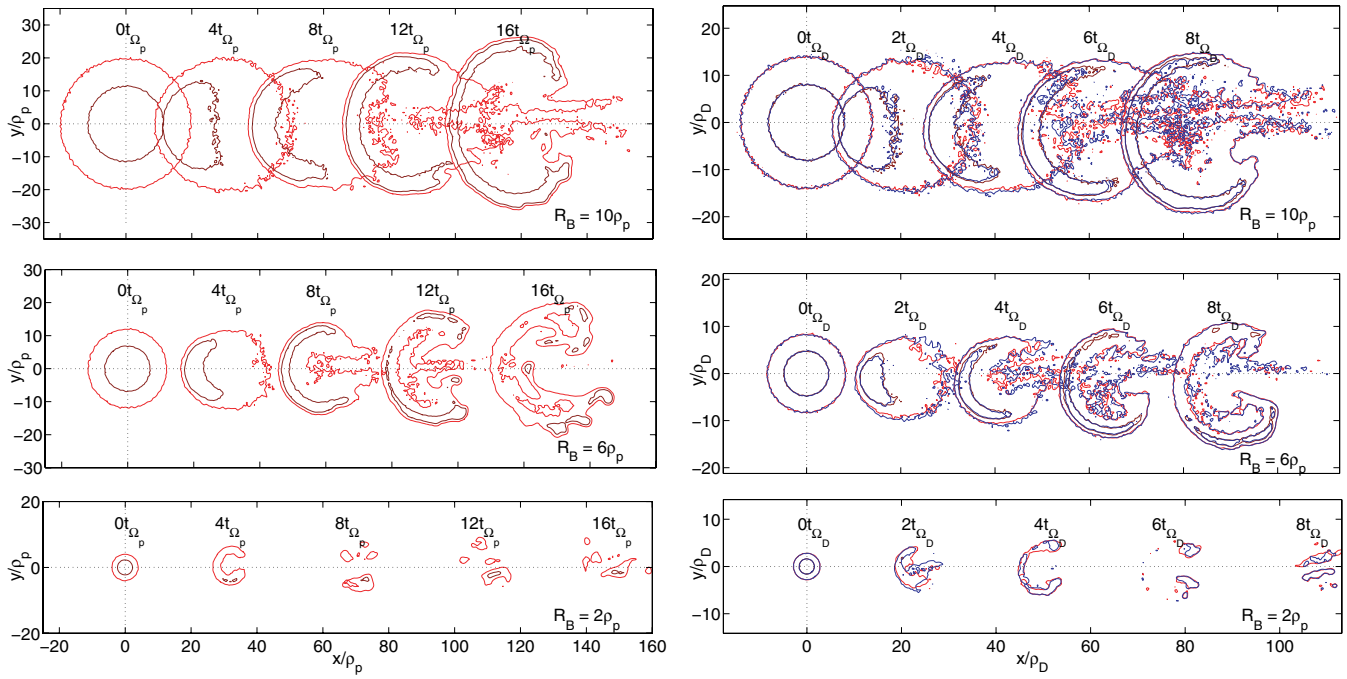

Figure 2. Number density contours for proton plasma blobs (left) and D–T plasma blobs (right) with initial radii 10, 6 and 2 ρ_p (top to bottom). Contours are displayed for number densities of $1.5n_0$ (light) and $3n_0$ (dark) at regular $4t_{\Omega_p}$ time intervals. For the D–T blobs, contours are given for both deuterons (red) and tritons (blue). Dotted lines mark the initial position of the blobs. These contours display the evolution of the blobs, including advection with the background flow, generation of Kelvin–Helmholtz instability on the lower edge, deflection of blobs in the $-y$ direction, and the shorter lifetime of smaller blobs. These figures present the evolution of the blobs in their initial rest frame.

background flow which interacts self-consistently with the blob. The motional electric field $\boldsymbol{E} = -\boldsymbol{u}_{\text{flow}} \times \boldsymbol{B}$ present in the flow imposes a potential difference across the blob, as shown in figure 1.

Simulations are performed for proton plasma blobs with initial radii R_B ranging from 1–10ρ_p, and also, for the first time, for 50 : 50 mix deuterium–tritium (D–T) plasma blobs of the same size. The evolution of both proton and D–T blobs is shown in figure 2. Large blobs for which $R_B \gg \rho_p$, as in the upper sections of figure 2, are advected with the background flow and develop internal, antisymmetric vortices as observed in [44]. Kelvin–Helmholtz instability develops on the lower edge of these larger blobs, creating corrugated structures at late times, visible at $16t_{\Omega_p}$ for the proton blob of radius $6\rho_p$. This instability grows more quickly on the lower edge than the upper edge as a result of finite Larmor radius symmetry breaking [9, 23]. Smaller blobs, for which $R_B \sim \rho_p$ so that kinetic effects are more important, develop stronger asymmetries in y, and are deflected in the $-y$ direction as a result of ion pick-up as in [34]. Small blobs also display a reduced lifetime, breaking up on shorter timescales.

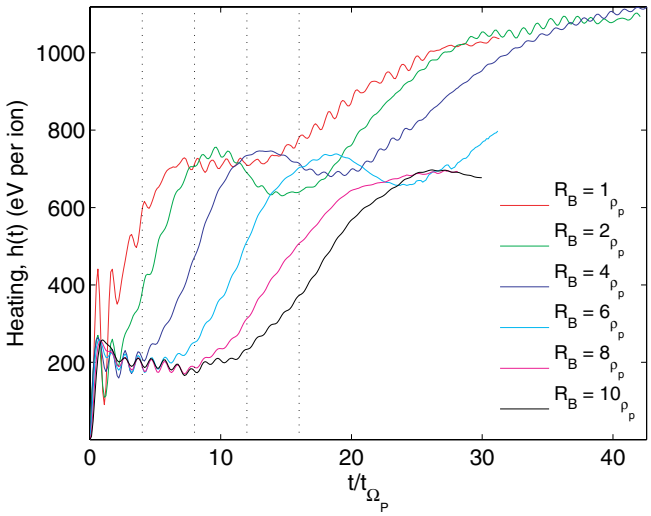

Figure 3. Energy transfer to blob ions plotted for proton plasma blobs of varying radii, calculated by integration of $\boldsymbol{J} \cdot \boldsymbol{E}$ for blob ions in space and time. Dotted lines mark times at which number density contours are plotted in figure 2. The more rapid heating displayed for smaller blobs implies a greater ability of smaller blobs to heat the plasma.

3. Heating

Let us focus on how ion heating varies with blob size. We can obtain from the simulations the rate at which any subset of ions gains energy by calculating $\boldsymbol{J}_\alpha \cdot \boldsymbol{E}$, where $\boldsymbol{J}_\alpha$ is the current carried by that subset of ions. Hence we can calculate the cumulative energy transfer from background ions to the blob ions via the electromagnetic fields as a function of time, by integrating over the simulation domain and time:

$$h(t) = \frac{1}{N_B} \int_0^t \iint_D \boldsymbol{J}_B \cdot \boldsymbol{E} \, \mathrm{d}x \, \mathrm{d}y \, \mathrm{d}t, \qquad (1)$$

where N_B is the total number of particles originating in the blob, D is the full simulation domain and $\boldsymbol{J}_B$ is the current

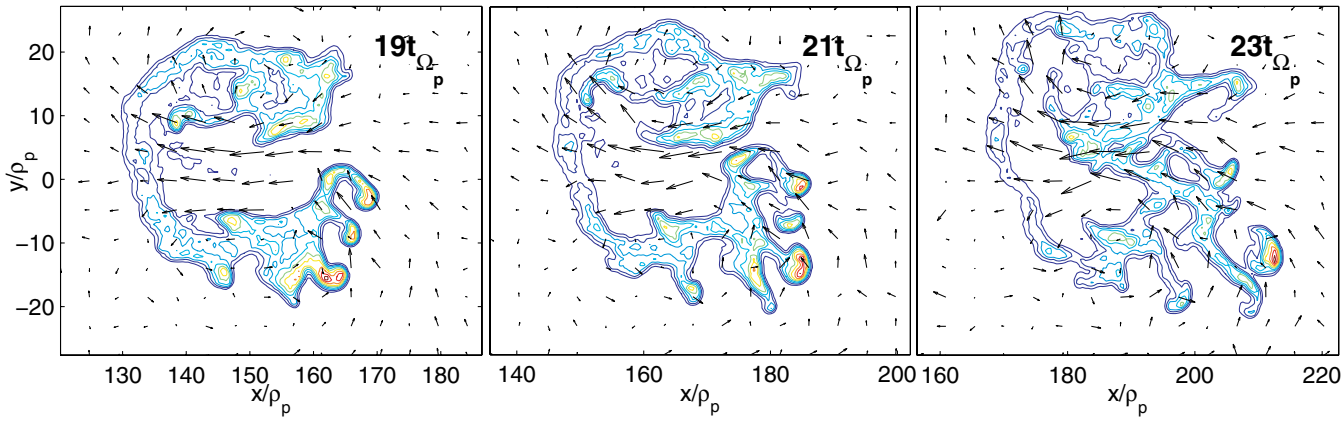

Figure 4. Evolution of a proton plasma blob of initial radius $6\rho_p$ during the time interval (see figure 3) associated with the cooling of blob ions. Number density contours are displayed with arrows representing the velocity field in the background flow frame. The colour scale indicates contour sequence from low (blue) to high (red). The interaction between the two coalescing high density regions at the downstream edge leads to disruption of the blob's vortex structure and loss of momentum of blob ions in that region.

density for the blob ions. This heating per blob ion $h(t)$ is plotted in figure 3 for proton plasma blobs of varying initial radii. All the curves show net heating with $h(t)$ increasing with t and small oscillations at the gyro-period. Importantly, there is a clear trend in the heating rate, which increases as blob size decreases. There is also a trend in the time at which significant heating starts. At middle times, the two high density regions of the blob formed in the upper and lower vortices interact at the downstream side, leading to a temporary plateau or reduction in heating as blob ions in that region lose momentum. This period of evolution is displayed in figure 4.

Figure 5 examines this heating effect for 50 : 50 mix D–T plasma blobs, relevant to burning fusion plasmas. There are now two populations of singly charged blob ions with different gyro-radii. We gain insight into the underlying heating process by normalizing the heating function per ion, $h(t)$, to particle mass m_D and m_T for their respective species. This normalized heating function is plotted in the main panel of figure 5 for D–T plasma blobs of radius ρ_p and $10\rho_p$, with the heating function $h(t)$ inset. As in the proton plasma case, the ions in smaller D–T blobs are heated faster, however the energy increase for the tritium population is larger than for deuterium in the same blob. Once normalized, we find close correspondence between the D and T populations—the only variation is in small oscillations on their respective gyro-periods. Therefore the heating scales with a factor common to both deuteron and triton populations.

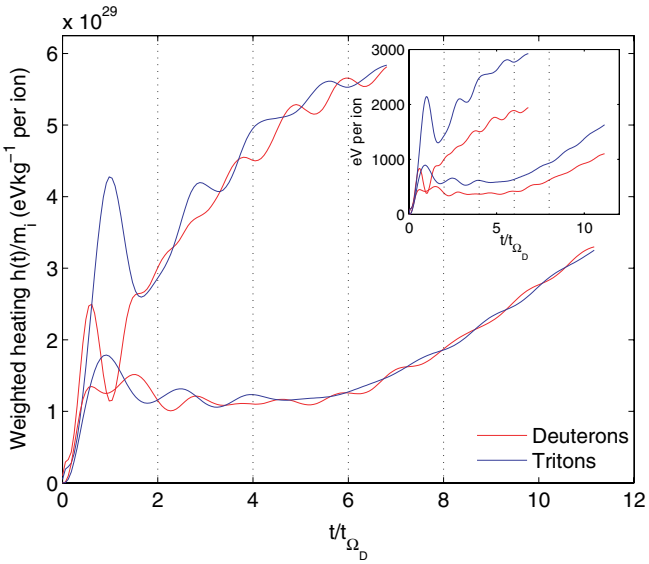

Figure 5. Energy transfer to blob ions in 50 : 50 mixed D–T plasma blobs of radius $1\rho_p$ (upper curves) and $10\rho_p$ (lower curves), normalized by particle mass; and inset with the energy transfer per ion as given in figure 3. Dotted lines mark times at which number density contours are plotted in figure 2. The correspondence between mass-normalized energy curves for deuteron and triton species demonstrates that the heating effect scales with a factor common to both species.

4. Momentum transfer

To investigate the mechanism for heating, we plot individual ion trajectories in figure 6. For blobs of radius $R_B \gg \rho_p$, the dynamics is fluid-like and heating can occur by momentum transfer around perturbations at the shear boundary between stationary blob plasma and flowing background plasma. For these larger blobs, a vortex pair forms, which would be antisymmetric in the fluid limit. Here, however, finite Larmor radius symmetry breaking causes the lower vortex to expand to a larger size than the upper vortex. The Kelvin–Helmholtz instability, which develops from perturbations on the shear boundary of these vortices, grows faster on the lower edge. These asymmetric vortex cells can be seen in the ion trajectories, as in the left of figure 6, which displays trajectories for particles initialized in the blob and background populations. Background ions deflect around the blob at the upstream edge, with a stagnation point along the line of symmetry, and blob ions follow the streamlines of internal vortices.

For blobs of radius $R_B \sim \rho_p$, figure 6 shows that the primary mechanism of momentum transfer is ion pick-up at the upstream edge of the blobs. To see this, consider two frames of reference: frame 1 in which the background plasma is stationary, with the blob plasma moving with speed v in the $-x$ direction; and frame 2 in which the background

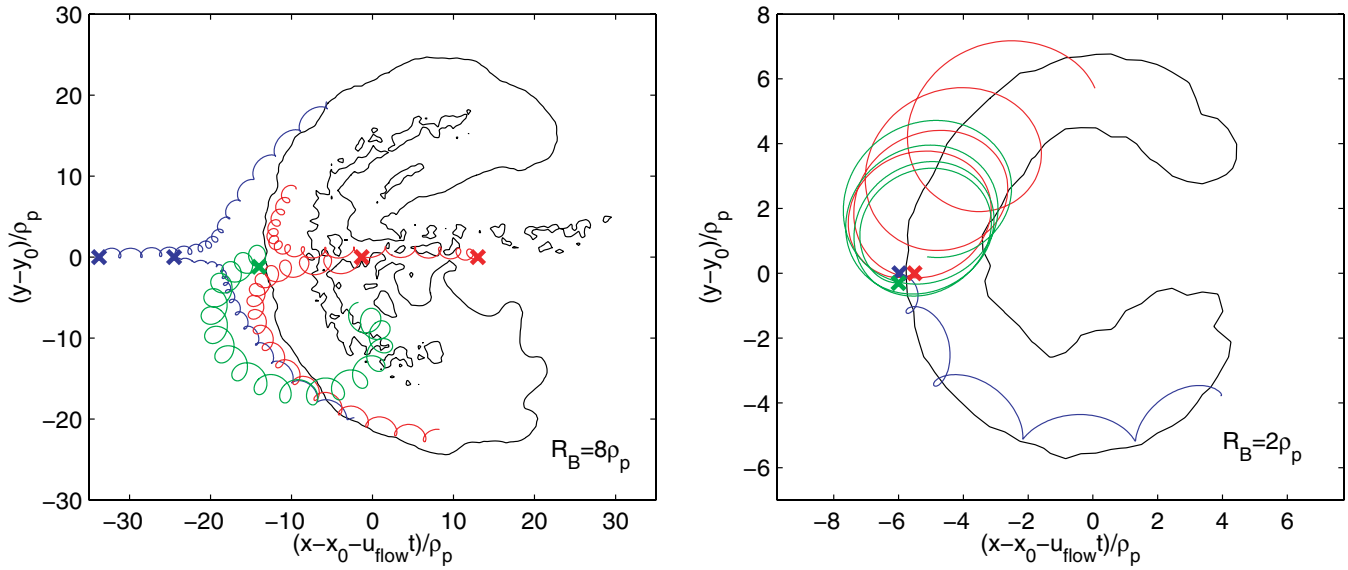

Figure 6. Ion trajectories plotted in the frame of reference of the blob, for blobs of initial radius $8\rho_p$ (left) and $2\rho_p$ (right). Initial positions of the ions are marked with an 'x'. For the larger blob, ions originating in both the blob (red) and the flow (blue) trace the streamlines of antisymmetric vortex cells formed on the upper and lower halves of the blob. For the smaller blob, an ion originating in the blob (red) is shown to pick-up in the flow and deflect in the $+y$ direction with relatively large gyro-radius, while an ion originating in the flow (blue) is deflected in the $-y$ direction with thermal gyro-radius. An additional blob ion is shown with a green trajectory in both cases, originating below the line of symmetry in the y-direction. This (green) ion is deflected in the $+y$ direction in the small blob, and the $-y$ direction in the large blob.

plasma is flowing with velocity $\boldsymbol{u}_{\rm flow} = -\boldsymbol{v}$ and the blob is stationary. A test particle in frame 1 which gyrates around the perpendicular magnetic fields lines will, in frame 2, execute a cycloid trajectory. This motion is consistent with the transformed electromagnetic fields, which in the non-relativistic case are:

$$\boldsymbol{B}_2 = \boldsymbol{B}_1, \tag{2}$$

$$\boldsymbol{E}_2 = \boldsymbol{E}_1 - \boldsymbol{v} \times \boldsymbol{B}_1, \tag{3}$$

where $\boldsymbol{E}_2$ is the motional electric field, present in the background of our simulations. Particles which are stationary in frame 2, i.e. those initialized in the blob, are accelerated by this motional electric field if they leave the spatial region that is dominated by blob ions and enter the background flowing plasma. This acceleration occurs in the direction of $\boldsymbol{E}_2$ and leads to momentum gain of the blob ions in the $\boldsymbol{v} \times \boldsymbol{B} = -\boldsymbol{u}_{\rm flow} \times \boldsymbol{B}$ direction, corresponding to the $+y$ direction in the simulations. Accelerated ions are said to have been 'picked-up' by the background flow, and execute a cycloidal trajectory in the direction of the $\boldsymbol{E} \times \boldsymbol{B}$ background flow, with relatively large gyro-radius $u_{\rm flow}/\Omega_{\rm i}$ and thermal velocity $u_{\rm flow}$. The momentum transfer which occurs between blob and background ions as a result of this mechanism can be seen by writing the ion momentum equation for a species α [34]:

$$m_\alpha n_\alpha \frac{{\rm D}\boldsymbol{v}_\alpha}{{\rm D}t} = e n_\alpha u_{\rm flow} \left(\frac{\boldsymbol{v}_\alpha}{u_{\rm flow}} - \frac{1}{n} \sum_{\alpha'} n_{\alpha'} \frac{\boldsymbol{v}_{\alpha'}}{u_{\rm flow}} \right) \times \boldsymbol{B},$$
$$+ \frac{n_\alpha}{n} \left(\boldsymbol{J} \times \boldsymbol{B} - \nabla \cdot \underline{\underline{P_{\rm e}}} \right), \tag{4}$$

where $\boldsymbol{v}_\alpha$ represents the fluid velocity field for species α, and total number density $n = \sum_{\alpha'} n_{\alpha'}$. The second term on the rhs is familiar in the fluid interpretation. The first term represents a symmetry breaking, present only in spatially inhomogeneous regions in which there is a difference between the mean velocities of different populations of ions. In the present case, these populations are the ions originating in the blob and those from the background plasma. This symmetry breaking term depends on particle velocity, displayed here as a fraction of the background fluid velocity $\boldsymbol{v}_\alpha/u_{\rm flow}$. Hence momentum gain resulting from this term scales with relative particle velocities and therefore background flow speed, but not with particle mass, as manifest in figure 5. The symmetry breaking term tends to zero as $\boldsymbol{v}_{\alpha'} \to \boldsymbol{v}_\alpha$, which is the fluid limit.

This mechanism [9] is a major contributor to finite Larmor radius symmetry breaking in the blobs. It can be seen in the individual ion trajectories in figure 6, which displays the $-y$ deflection of a typical background flow ion with thermal gyro-radius $\rho_{\rm p}$, and the $+y$ deflection of a blob ion displaying pick-up with a much larger gyro-radius. For blobs of radius $R_{\rm B} \sim \rho_{\rm p}$, the $+y$ deflection is seen even for blob ions originating below the line of symmetry.

5. Conclusions

Ion gyro-scale blobs, as simulated here, are not easily resolved by current tokamak diagnostics. They constitute a population of structures which is likely to exist, but whose number and distribution are unknown. Our simulations show that heating proceeds at a faster rate ${\rm d}h/{\rm d}t$ for smaller, un-resolvable blobs. The principal mechanisms behind the heating have been inferred from normalized results for D–T plasma blobs: in the kinetic case $R_{\rm B} \sim \rho_{\rm p}$, pick-up ions are accelerated on the

upstream edge of the blob, and in the fluid case $R_B \gg \rho_p$, momentum transfer occurs at the shear boundary between the blob and background plasmas. The total heating generated by blobs during their dwell time in the plasma τ is thus $\tau\, \mathrm{d}h/\mathrm{d}t$ which implies, for a dwell time independent of blob size, that smaller, ion gyro-scale blobs heat the plasma more than larger ones. These results indicate that the full ion kinetics of an observationally un-resolvable population of small blobs may be important in determining energy flow through and within the edge plasma in fusion experiments.

Acknowledgments

This work was part-funded by the EPSRC and the RCUK Energy Programme under grant EP/I501045 and the European Communities under the contract of Association between EURATOM and CCFE. The views and opinions expressed herein do not necessarily reflect those of the European Commission. We also thank the EPOCH development team for their work on the PIC code adapted for this research.

References

[1] Boedo J A *et al* 2003 *Phys. Plasmas* **10** 1670
[2] Grulke O, Terry J L, Labombard B and Zweben S J 2006 *Phys. Plasmas* **13** 012306
[3] Myra J R, D'Ippolito D A, Stotler D P, Zweben S J, Leblanc B P, Menard J E, Maqueda R J and Boedo J 2006 *Phys. Plasmas* **13** 092509
[4] Nold B, Conway G D, Happel T, Müller H W, Rohde V, Stroth U and the ASDEX Upgrade Team 2010 *Plasma Phys. Control. Fusion* **52** 065005
[5] Kirk A *et al* 2006 *Plasma Phys. Control. Fusion* **48** B433
[6] Podestà M, Fasoli A, Labit B, Furno I, Ricci P, Poli F M, Diallo A, Müller S H and Theiler C 2008 *Phys. Rev. Lett.* **101** 045001
[7] Angus J R, Umansky M V and Krasheninnikov S I 2012 *Phys. Rev. Lett.* **108** 215002
[8] Kukushkin A S, Pacher H D, Pacher G W, Janeschitz G, Coster D, Loarte A and Reiter D 2003 *Nucl. Fusion* **43** 716
[9] Gingell P W, Chapman S C, Dendy R O and Brady C S 2012 *Plasma Phys. Control. Fusion* **54** 065005
[10] Krasheninnikov S I 2011 *Plasma Phys. Control. Fusion* **53** 074017
[11] Krasheninnikov S I 2001 *Phys. Lett.* A **283** 368
[12] D'Ippolito D A, Myra J R and Krasheninnikov S I 2002 *Phys. Plasmas* **9** 222
[13] Aydemir A Y 2005 *Phys. Plasmas* **12** 062503
[14] Russell D A, D'Ippolito D A, Myra J R, Nevins W M and Xu X Q 2004 *Phys. Rev. Lett.* **93** 265001
[15] Garcia O E, Bian N H, Naulin V, Nielsen A H and Rasmussen J J 2005 *Phys. Plasmas* **12** 090701
[16] Yu G Q, Krasheninnikov S I and Guzdar P N 2006 *Phys. Plasmas* **13** 042508
[17] Higgins D, Hnat B, Kirk A, Tamain P, Ben Ayed N and the MAST Team 2012 *Plasma Phys. Control. Fusion* **54** 015002
[18] Park W, Belova E V, Fu X Z, Strauss H R and Sugiyama L E 1999 *Phys. Plasmas* **6** 1796
[19] Madsen J, Garcia O E, Stærk Larsen J, Naulin V, Nielsen A H and Rasmussen J J 2011 *Phys. Plasmas* **18** 112504
[20] Yu G Q and Krasheninnikov S I 2003 *Phys. Plasmas* **10** 4413
[21] Krasheninnikov S I, D'Ippolito D A and Myra J R 2008 *J. Plasma Phys.* **74** 679
[22] D'Ippolito D A, Myra J R and Zweben S J 2011 *Phys. Plasmas* **18** 060501
[23] Nagano H 1979 *Planet. Space Sci.* **27** 881
[24] Hasegawa H, Fujimoto M, Phan T-D, Rème H, Balogh A, Dunlop M W, Hashimoto C and TanDokoro R 2004 *Nature* **430** 755
[25] Sundkvist D, Krasnoselskikh V, Shulka P K, Vaivads A, Ardrè M, Buchert S and Rème H 2005 *Nature* **436** 825
[26] Sundkvist D and Bale S D 2008 *Phys. Rev. Lett.* **101** 065001
[27] Nykyri K and Otto A 2001 *Geophys. Res. Lett.* **28** 3565
[28] Smets R, Belmont G, Delcourt D and Rezeau L 2007 *Ann. Geophys.* **25** 271
[29] Pritchett P L and Mozer F S 2011 *J. Geophys. Res.* **116** A04215
[30] Lipatov A S, Sauer K and Baumgärtel K 1997 *Adv. Space Res.* **20** 279
[31] Bagdonat T and Motschmann U 2002 *Earth Moon Planet* **20** 305
[32] Motschmann U and Kürt E 2006 *Space Sci. Rev.* **122** 197
[33] Valenzuela A, Haerendel G, Foeppl H, Melzner F and Neuss H 1986 *Nature* **320** 700
[34] Chapman S C and Dunlop M W 1986 *J. Geophys. Res.* **91** 8051
[35] Brecht S H and Ferrante J R 1991 *J. Geophys. Res.* **96** 11209
[36] Sauer K, Bogdanov A and Baumgartel K 1995 *Adv. Space Res.* **16** 153
[37] Brecht S H 1997 *J. Geophys. Res.* **102** 4743
[38] Shimazu H 2002 *J. Geophys. Res.* **106** 8333
[39] Terada N, Machida S and Shinagawa H 2002 *J. Geophys. Res.* **107** 1471
[40] Simon S and Motschmann U 2009 *Planet. Space Sci.* **57** 2001
[41] Kallio E, Liu K, Jarvinen R, Pohjola V and Janhunen P 2010 *Icarus* **206** 152
[42] Winske D, Yin L, Omidi N, Karimabadi H and Quest K 2003 *Space Plasma Simulation, Lecture Notes in Physics* vol 615 (Berlin: Springer) p 136
[43] Hewett D W 1994 *Comput. Phys. Commun.* **84** 243
[44] Katz N, Egedal J, Fox W, Le A and Porkolab M 2008 *Phys. Rev. Lett.* **101** 015003